



Norwegian University of  
Science and Technology

# Zinc Oxide Nanolaser

Photoluminescence spectroscopy and optical pumping of zinc oxide nanowires

**Filip August Heitmann**

Master of Science in Electronics

Submission date: February 2012

Supervisor: Helge Weman, IET

Co-supervisor: Lyubomir Ahtapodov, IET



# Zinc Oxide Nanolaser

Photoluminescence spectroscopy and optical pumping of zinc oxide nanowires

Written by Filip August Heitmann

Completed: Autumn 2011  
Handed in: February 14, 2012

Supervisor: Professor Helge Weman, IET

FACULTY OF INFORMATION TECHNOLOGY,  
MATHEMATICS AND ELECTRONICS

---



# Problem description

The project will focus on photoluminescence (PL) spectroscopy and optical pumping of single ZnO nanowires (NW) with the aim of realizing ZnO nanolasers for the first time at NTNU. The samples and devices will also be characterized with time-resolved PL spectroscopy. Both NWs grown at NTNU and at collaborators universities abroad will be studied. For this purpose a dedicated setup in the Nanophotonics lab built and adapted into the already existing setup within a previous project by the same student will be used. State of the art high-power lasers and other optical equipment will be utilized. Also, new equipment (flexible harmonic generator unit and streak camera) will be set in operation and involved in experimental work for the first time in the lab. Additionally, GaAs/AlGaAs/ZnO core/multishell nanowires will be examined in PL spectroscopy at different excitation wavelengths. In order to assess the potential of such NWs for applications such as NW solar cells, both doped and undoped NWs will be studied.

# Abstract

This Master's thesis is a continuation of the specialization project I did during the spring of 2011. The goal of said project was to set up a system for UV-photoluminescence experiments in the Nanophotonics laboratory at the Department of Electronics and Telecommunications at NTNU, and conduct photoluminescence spectroscopy measurements on different zinc oxide nanostructures, including GaAs/AlGaAs/ZnO core/multishell nanowires. This thesis involves studying zinc oxide nanowires using both a continuous wave and pulsed ultraviolet laser light, and the final goal is to optically excite these nanowires so they achieve lasing. Using a Tsunami Ti:sapph mode-locked tunable laser and a flexible harmonic generator, laser pulses with a pulse duration of 2 ps could be generated at wavelengths around 300 nm, at a power of around 5 mW. At this power, some of the wires showed possible signs of optical gain, but since it was not possible to apply more power to the wires, this could not be confirmed. If there had been enough time, both low temperature measurements and time-resolved spectroscopy, using a streak camera, would have been performed.

# Preface

This Master's thesis is a continuation of the specialization project I did during the spring of 2011. The goal of said project was to set up a system for UV-photoluminescence experiments in the Nanophotonics laboratory at the Department of Electronics and Telecommunications at NTNU, and conduct photoluminescence spectroscopy measurements on different zinc oxide nanostructures.

Both the specialization project and this Master's thesis is a part of the research on nanowire structures for applications in future-generation solar cells conducted by the Nanowire group, led by professor Helge Weman, at the Dept. of Electronics and Telecommunications.

I would want to thank Lyubomir Ahtapodov for helping me with both my specialization project and this thesis, providing training for me in the lab, being responsible for the purchase of all optical equipment required, and answering any questions I might have had during the time we worked together.

I would also like to thank professor Helge Weman for providing me with this project, including me in the Nanowire research group, providing me with background material, and giving valuable feedback during the process of writing this thesis.

A special thanks goes out to all the members of the Nanowire research group for their feedback and discussions during the weekly group meetings, to professor Sang Wook Lee at Konkuk University for providing the nanowires for this thesis, and to Christian Weigand for providing the nanostructures for the specialization project.

# Contents

<b>1</b>	<b>Introduction</b>	<b>1</b>
<b>2</b>	<b>Theory</b>	<b>2</b>
2.1	Chemical Vapor Deposition . . . . .	2
2.2	Photoluminescence . . . . .	3
<b>3</b>	<b>Experimental</b>	<b>4</b>
3.1	Optical system setup . . . . .	4
3.1.1	Pump laser . . . . .	4
3.1.2	Tsunami mode-locked Ti:sapphire laser . . . . .	4
3.1.3	Flexible Harmonic Generator . . . . .	5
3.1.4	Helium-cadmium UV laser . . . . .	5
3.2	Dispersion of wires . . . . .	5
3.3	Continuous wave excitation . . . . .	6
3.4	Setup of the pulsed laser system . . . . .	6
3.5	Pulsed laser excitation . . . . .	6
<b>4</b>	<b>Results and discussion</b>	<b>9</b>
4.1	Continuous wave excitation . . . . .	9
4.2	Pulsed laser excitation . . . . .	11
<b>5</b>	<b>Conclusion</b>	<b>13</b>
<b>6</b>	<b>Appendix</b>	<b>15</b>
6.1	Power dependence and standard deviation . . . . .	15
6.2	Photoluminescence spectroscopy measurements . . . . .	19
6.2.1	Continuous wave measurements . . . . .	19
6.2.2	Pulsed laser measurements . . . . .	24

# List of abbreviations

<b>UV</b>	Ultraviolet
<b>PL</b>	Photoluminescence
<b>PLD</b>	Pulsed laser deposition
<b>DPSS</b>	Diode-pumped solid state (laser)
<b>Nd:YVO<sub>4</sub></b>	Neodymium-doped yttrium orthovanadate
<b>AlGaAs</b>	Aluminium gallium arsenide
<b>LBO</b>	Lithium triborate
<b>Ti:sapph</b>	Titanium-doped sapphire (Al <sub>2</sub> O <sub>3</sub> )
<b>FWHM</b>	Full width at half maximum
<b>Bi-fi</b>	Birefringent filter
<b>GTI</b>	Gires-Tournois Interferometer
<b>GVD</b>	Group velocity dispersion
<b>BBO</b>	Beta-barium borate
<b>CW</b>	Continuous wave
<b>HeCd</b>	Helium cadmium
<b>FHG</b>	Flexible harmonic generator

# List of Tables

6.1	NW1 power dependence, 310 nm excitation, 60 s average . . . . .	15
6.2	NW2 power dependence, 310 nm excitation, 60 s average . . . . .	15
6.3	NW3 power dependence, 310 nm excitation, 60 s average . . . . .	15
6.4	NW4 power dependence, 310 nm excitation, 60 s average . . . . .	16
6.5	NW1 power dependence, 300 nm excitation, 60 s average . . . . .	17
6.6	NW2 power dependence, 300 nm excitation, 60 s average . . . . .	17
6.7	NW3 power dependence, 300 nm excitation, 60 s average . . . . .	17
6.8	NW4 power dependence, 300 nm excitation, 60 s average . . . . .	18

# List of Figures

2.1	Plasma-enhanced CVD . . . . .	3
2.2	$\mu$ -Photoluminescence spectroscopy setup . . . . .	3
3.1	SEM image of a dispersed wire . . . . .	5
3.2	Transmittance vs Wavelength for Oxygen and Water Vapor . . . . .	7
3.3	Tsunami femtosecond tuning curves for broadband optics when pumped by the various Millennia diode-pumped lasers shown. . . . .	7
3.4	FHG tuning curve, $3\omega$ , 10 W pump laser . . . . .	8
4.1	PL spectrum of NW1, continuous wave . . . . .	9
4.2	Optical image of excitation, NW2 . . . . .	10
4.3	Power dependence, NW2 . . . . .	10
4.4	Pulsed laser illumination, 310nm, NW2 . . . . .	11
4.5	Pulsed laser illumination, 300nm, NW4 . . . . .	12
4.6	Power dependence, 300nm, NW4 . . . . .	12
6.1	NW1, 11/11/11 . . . . .	19
6.2	NW2, 11/11/11 . . . . .	19
6.3	NW3, 11/11/11 . . . . .	20
6.4	NW4, 11/11/11 . . . . .	20
6.5	NW1 bottom, 19/01/12 . . . . .	21
6.6	NW1 center, 19/01/12 . . . . .	21
6.7	NW1 top, 19/01/12 . . . . .	22
6.8	NW2 bottom, 19/01/12 . . . . .	22
6.9	NW2 center, 19/01/12 . . . . .	23
6.10	NW2 top, 19/01/12 . . . . .	23
6.11	NW1, 310 nm excitation, 27/01/12 . . . . .	24
6.12	NW2, 310 nm excitation, 27/01/12 . . . . .	24
6.13	NW3, 310 nm excitation, 27/01/12 . . . . .	25
6.14	NW4, 310 nm excitation, 27/01/12 . . . . .	25

# Chapter 1

## Introduction

Zinc oxide has become an interesting material within the field of optoelectronics. It has a wide direct band gap(3.37 eV), and a exciton binding energy of 60 meV at room temperature, the latter allowing the material to be optically pumped and achieve lasing in room temperature[1],[2]. In addition, zinc oxide is a promising candidate for use in next-generation solar cells. The Nanowire research group at the Dept. of Electronics and Telecommunications at NTNU is currently exploring the potential of GaAs nanowires for this specific purpose. Since ZnO is transparent to visible light, and intrinsically n-doped[3], it is possible that a GaAs/AlGaAs/ZnO core-multishell nanowire could be implemented as a photovoltaic p-n junction.

# Chapter 2

## Theory

### 2.1 Chemical Vapor Deposition

Chemical vapor deposition is a common method for depositing a high-quality thin film to a substrate. The deposition occurs due to chemical reactions taking place on or close to the substrate. Reactants are introduced into reactor, and, depending on the reactants, a reaction is caused by for example heat, irradiation or oxidation.

CVD reaction steps, taken from [4]:

1. **Gas transport to deposition zone:** Mass transport of gas in the main gas flow region from the reactor inlet to the deposition zone of the wafer.
2. **Formation of film precursors:** Gas-phase reactions leading to the formation of the film precursors (initial atoms and molecules that will constitute the film) and by-products.
3. **Film precursors at wafer:** Mass transport of the film precursors to the wafer growth surface.
4. **Precursor adsorption:** Adsorption (binding) of film precursors to the surface.
5. **Precursor diffusion:** Surface diffusion of film precursors to the film growth sites.
6. **Surface reactions:** Surface chemical reactions leading to film deposition and by-products.
7. **By-product removal from surface:** Desorption (removal) of the by-products of the surface reactions.
8. **By-product removal from reactor:** Mass transport of the by-products in the bulk gas-flow region away from the deposition zone and towards the reactor exit.

Several variations of CVD systems exist, for example atmospheric and low-pressure CVD, as well as plasma-assisted and -enhanced CVD. Some of the advantages of a CVD reactor is fast and controllable (by adjusting reactant gas flow) deposition, the possibility to deposit on multiple wafers simultaneously, the possibility to introduce dopants, and its wide application range, being able to deposit various materials[4].

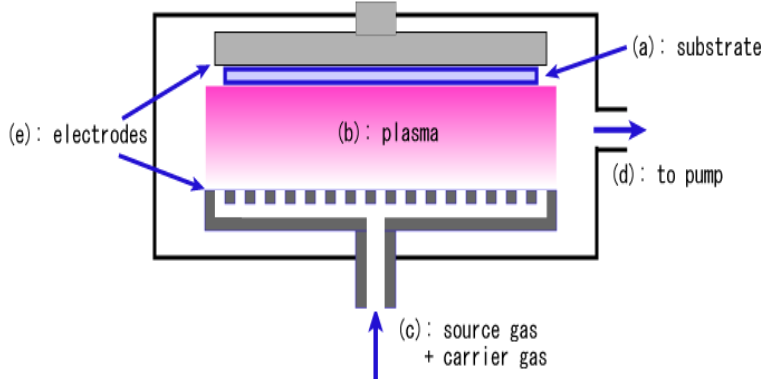


Figure 2.1: Plasma-enhanced CVD

## 2.2 Photoluminescence

Photoluminescence is the phenomenon of light emission from a material due to optical stimulation. The absorption of photons can excite a charge carrier in a semiconductor if the photon energy is larger than the energy band gap of the semiconductor, creating an electron-hole pair. When the electron-hole pair recombines, the charge carrier returns to its equilibrium state, the excess energy is released in the form of photons.

In a perfect crystal the recombination occurs almost instantly (within tens of nanoseconds) since the charge carrier is relaxed directly from the conduction energy band to the valence energy band, which results in a sharp peak in the emission spectrum. In reality, however, a crystal contains impurities or defects which traps the charge carrier at a certain energy level, resulting in a broader emission peak.

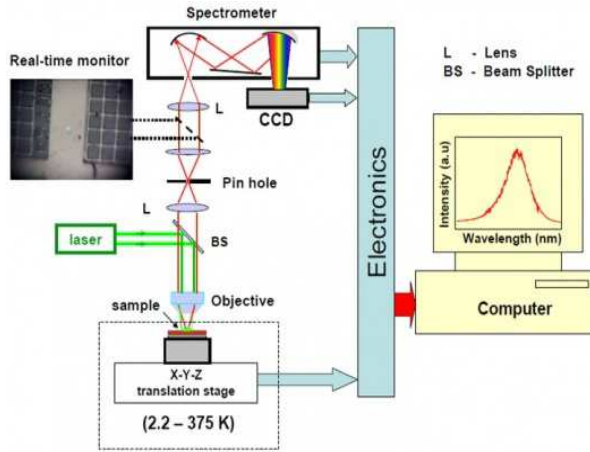


Figure 2.2:  $\mu$ -Photoluminescence spectroscopy setup

In a  $\mu$ -PL spectroscopy setup, the illumination beam and the PL emission travels along the same path through the focusing objective. Using beam splitters (or, as is the case in this thesis, a dichroic mirror), as seen in figure 2.2, the emission beam can be diverted to a spectrometer for measurement. Any reflected laser light traveling this path is blocked by a filter.

# Chapter 3

## Experimental

### 3.1 Optical system setup

#### 3.1.1 Pump laser

The pump laser used during the experiments is a Spectra-Physics Millennia Pro; a 6 W, 532 nm continuous-wave diode-pumped solid state(DPSS) laser. The laser operates by optically pumping a Nd:YVO<sub>4</sub> crystal using AlGaAs laser diodes emitting 808 nm infrared light. The excited neodymium ions in the Nd:YVO<sub>4</sub> crystal will achieve stimulated emission, producing laser light at a wavelength of 1064 nm. This output is converted to 532 nm laser light through second harmonic generation in a phase-matched, temperature-tuned lithium triborate (LBO) non-linear crystal. The power of the final 532 nm laser light is given by

$$P_{2\omega} \propto \frac{d_{eff}^2 P_{\omega}^2 l^2 [\Phi]}{A} \quad (3.1)$$

where  $d_{eff}$  is the effective nonlinear coefficient,  $P_{\omega}$  is the fundamental input power,  $l$  is the effective crystal length,  $[\Phi]$  is a phase-matching factor, and  $A$  is the cross-sectional area of the beam in the crystal.

#### 3.1.2 Tsunami mode-locked Ti:sapphire laser

The Spectra-Physics Tsunami mode-locked, tunable, titanium-doped sapphire (Ti:sapphire) solid-state laser, able to output a broad range of near infrared wavelengths. It can deliver a continuously tunable output from 690 nm to 1080 nm by using different overlapping mirror sets. The laser can produce ultrashort light pulses with a pulse widths (FWHM) in both the femtosecond and picosecond regime.

In this thesis the Tsunami was used in the picosecond configuration, which uses a birefringent filter (bi-fi) for tuning the wavelength. A bi-fi uses a Brewster window to filter out all but a narrow peak of the Ti:sapph's broad emission, allowing for a continuous wavelength selection. The pulse width is adjusted using a Gires-Tournois Interferometer (GTI). A GTI has negative group velocity dispersion, which compensates the positive GVD of the Ti:sapph crystal.

The Tsunami laser requires a pump laser, which in this case is the Millennia Pro.

### 3.1.3 Flexible Harmonic Generator

The Spectra-Physics GWU Flexible Harmonic Generator is able to generate second and third harmonics of the pulsed laser beam generated by the Tsunami laser.

The second order harmonic of the fundamental laser beam is generated in a beta-barium borate (BBO) non-linear optical crystal.

The third order harmonic is generated by spatial and temporal overlap of the fundamental and doubled beams in another non-linear crystal, resulting in frequency mixing.

### 3.1.4 Helium-cadmium UV laser

The Kimmon helium-cadmium (HeCd) metal vapor laser is used for the continuous wave measurements in this project. The laser operation wavelengths, namely 325 nm (UV) and 441.6 nm (blue), which can be individually selected using filters in the laser shutter. It emits 10 mW of 325 nm laser light, according to the data sheet (See appendix)

## 3.2 Dispersion of wires

The nanowires were grown by professor Sang Wook Lee at Konkuk University in Seoul, South Korea using chemical vapor deposition. Inspection of the wires through a scanning electron microscope shows that the wire diameter is about 500 nm, and the wire length varies between 10 to 25  $\mu\text{m}$ .

The nanowires were delivered in a ethanol solution, and therefore requiring dispersion on silicon dioxide substrates. Due to the low concentration of nanowires in the solution, the initial dispersions were unsuccessful. However, after performing multiple dispersions on on single substrate, optical inspection confirmed several nanowires were to be found on the substrate.

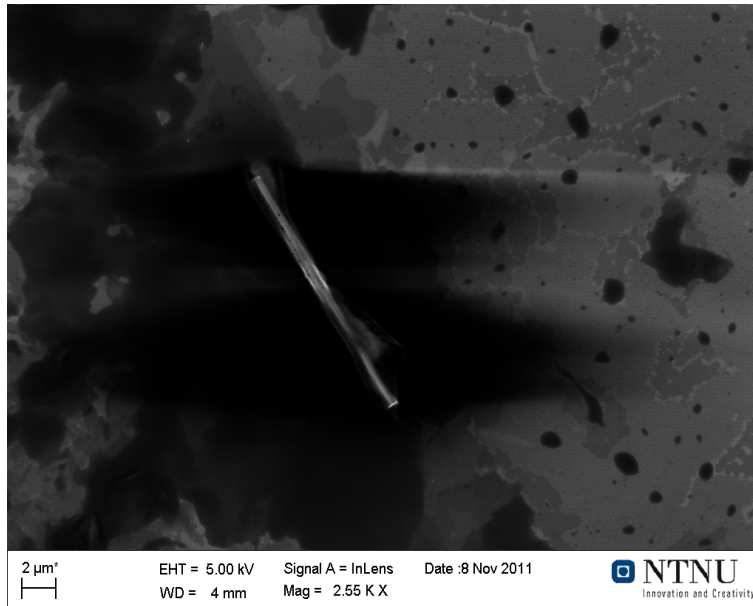


Figure 3.1: SEM image of a dispersed wire

### 3.3 Continuous wave excitation

In the specialization project preceding this thesis, carried out in the spring of 2011, a system for conducting ultraviolet measurements in the nanophotonics laboratory at the Dept. of Electronics and Telecommunications at NTNU was set up, using UV-enhanced mirrors and beam splitters.

The first round of continuous wave (CW) measurements was conducted to make sure the optical setup was still functional, as well as to verify proper PL emission from the nanowires.

Subsequent to optimizing the optical setup, i.e. maximizing the optical power delivered to the substrate and the PL emission power delivered to the spectroscopy detector, measurements at several illumination powers were conducted on the dispersed nanowires.

### 3.4 Setup of the pulsed laser system

In order to deliver pulsed UV laser light to the sample, both the Tsunami mode-locked laser and the GWU flexible harmonic generator had to be realigned and optimized. To achieve maximum optical power the the Tsunami had to be converted to picosecond pulse mode. This is done by moving the the prism pair used for femtosecond operation out of the beam path, and insert a birefringent filter and GTI (see section 3.1.2). The conversion to picosecond mode does not only increase the average power output from the Tsunami, but the broader pulses also increases the performance of the FHG compared to the femtosecond configuration.

The FHG had only been configured for second harmonic generation previously, therefore, in spite of extensive attempts to configure the FHG for frequency tripling, a service engineer was required to align the FHG properly.

To obtain the wavelength required for PL excitation, the Tsunami was tuned to around 900 nm, which corresponds to a third harmonic of around 300 nm.

### 3.5 Pulsed laser excitation

In the initial measurements using the pulsed laser there were some problems regarding the stability of the mode-locking. However, by purging the Tsunami laser with nitrogen gas, the stability increased noticeably. Oxygen and water vapor can cause a reduction in transmittance in the Tsunami, especially around 900 nm, as shown in figure 3.2.

The power delivered to the sample is affected by several factors. Firstly, the output power of the Tsunami depends on the selected wavelength, as shown in figure 3.3. Secondly, the performance of the FHG also varies at different wavelengths, as shown in figure 3.4. Lastly, the optics in the illumination path are specified for certain wavelengths, and the reflectivity will drop drastically at short (sub-300 nm) wavelengths (See appendix for mirror datasheets). Therefore, measurements at different wavelengths in this region were conducted to optimize the amount of power delivered to the sample.

Measurements of the wires were conducted at several different wavelengths and powers.

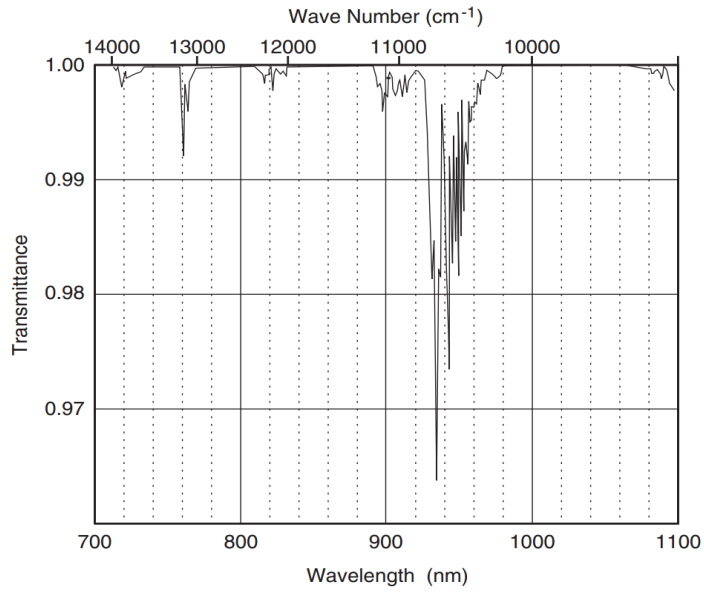


Figure 3.2: Transmittance vs Wavelength for Oxygen and Water Vapor

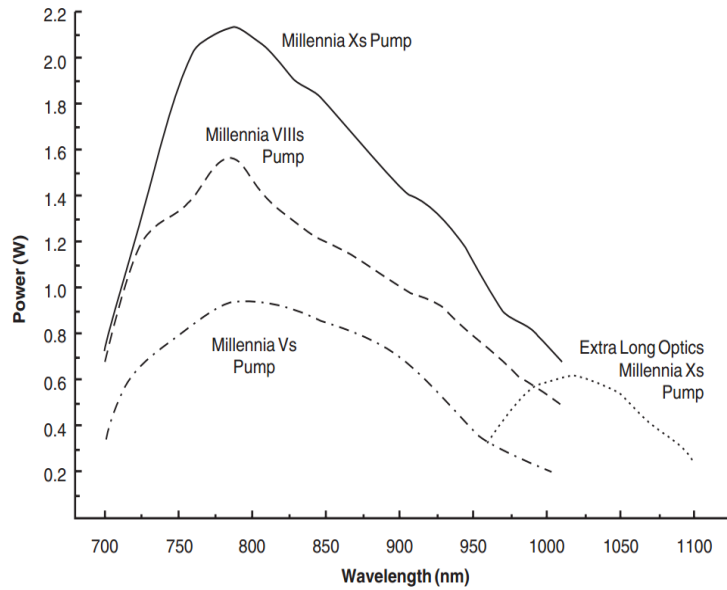


Figure 3.3: Tsunami femtosecond tuning curves for broadband optics when pumped by the various Millennia diode-pumped lasers shown.

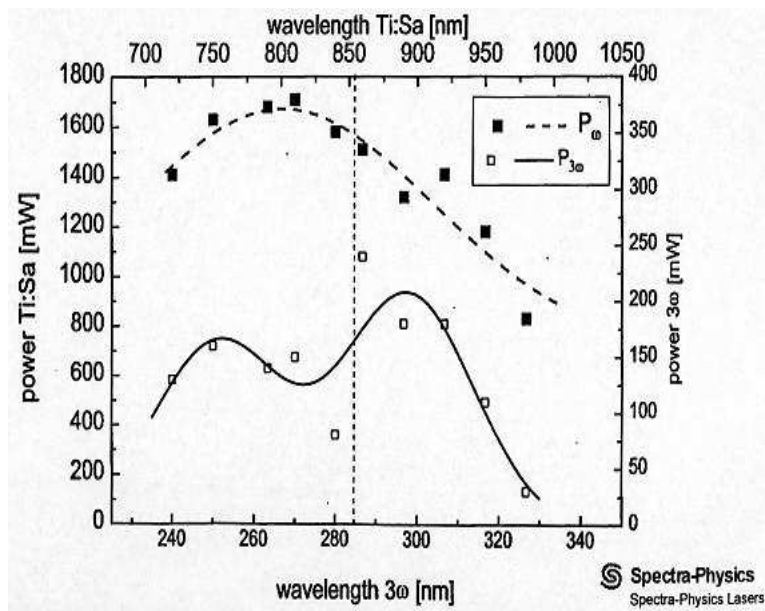


Figure 3.4: FHG tuning curve,  $3\omega$ , 10 W pump laser

# Chapter 4

## Results and discussion

### 4.1 Continuous wave excitation

As mentioned in section 3.1.4, the maximum output of the HeCd-laser was 10 mW of 325 nm light. Power measurements at the sample showed that about 6 mW of power reached the sample; the rest is absorbed or diffracted in the mirrors in the illumination path. Although the transmittance is not optimal, it is significantly better than the power dissipation prior to specialization project carried out in spring 2011. At that time only 1.2 mW of power reached the sample. By using UV-enhanced mirrors in the illumination path, high-quality ultra-broadband mirrors in the sample holder periscope (so UV, visible and IR measurements could be conducted without changing these mirrors), and a dichroic mirror instead of a beam splitter, the delivered laser power was increased to the current value.

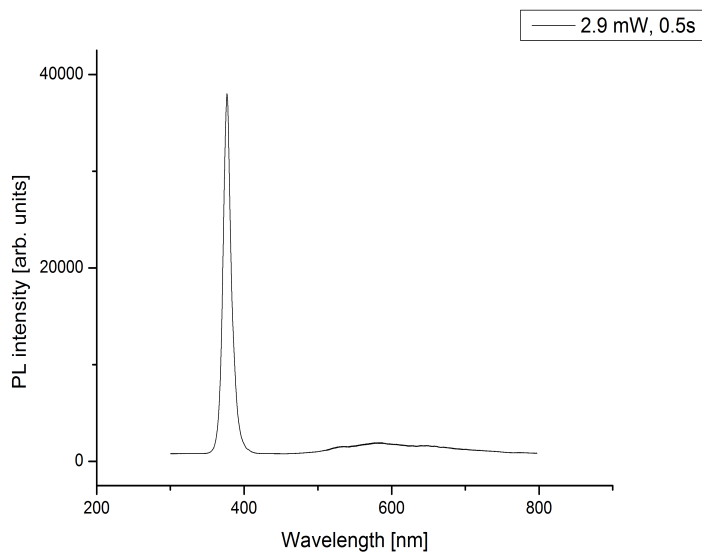


Figure 4.1: PL spectrum of NW1, continuous wave

The photoluminescence spectra of the different wires showed bright and narrow excitation peaks in most of the wires. Optical images of the excitation show indication of wave guidance through the nanowires, as shown in figure 4.2.



Figure 4.2: Optical image of excitation, NW2

Since the power of the emitted PL is given by

$$P = \int I \, dA \quad (4.1)$$

the ratio between illumination power and PL power, as shown in figure 4.3, is inconclusive. There is a possible indication of some optical gain, but no clear sign.

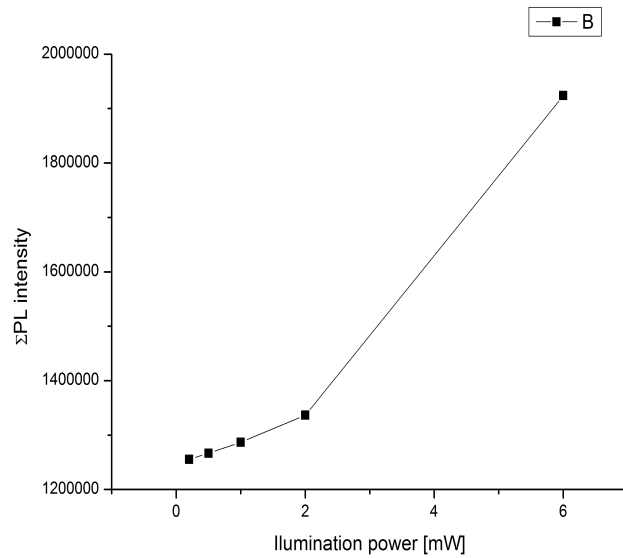


Figure 4.3: Power dependence, NW2

## 4.2 Pulsed laser excitation

The first measurements were performed using illumination light at 310 nm. Although the FHG provides less power at this wavelength than at slightly lower wavelengths, due to the drastic drop of reflectance in the mirrors in the illumination path at such low wavelengths, a compromise was found at 310 nm.

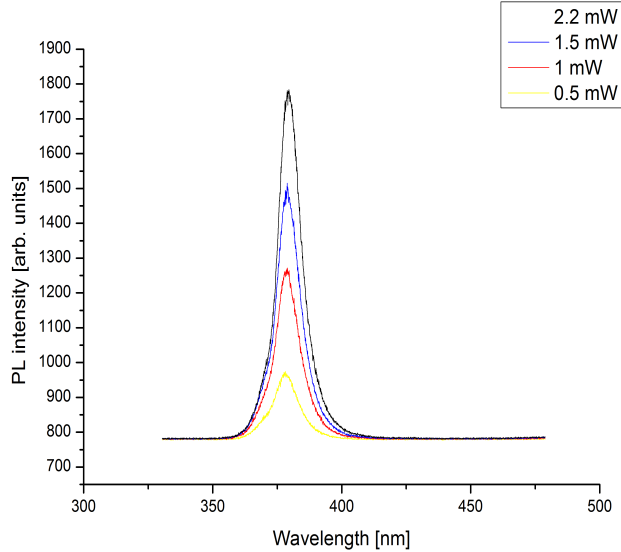


Figure 4.4: Pulsed laser illumination, 310nm, NW2

At this wavelength only 2.2 mW of power was delivered to the sample, and power was also varying noticeably (See table 6.3). Using nitrogen to purge the Tsunami laser, these power variations were reduced, and it also increased the stability of the pulsing. However, the PL emission was weak in all wires and not showing any indication of optical gain. An average power, measured over 60 s, is used instead of one specific power, due to these power variations. The measured powers and standard deviation is listed in section 6.1.

To try to increase the delivered power, the wavelength was reduced to 300 nm. After optimizing the Tsunami and FHG, the powers measured at the opening of the FHG and at the sample were around 11 and 5.5 mW, respectively, indicating that the dissipation for the pulsed 300 nm light and the continuous 325 nm light is comparable.

Unfortunately, an error occurred during the measurements, resulting in some of the PL data being corrupted. The measured PL peaks of the wires at different powers, in addition to average illumination power and standard deviation, are also listed in section 6.1. Nevertheless, one of the wires showed some indication of possible optical gain, as shown in 4.6.

An attempt to go even further down in wavelength, to around 286 nm, was performed, which required the mirrors in the sample holder periscope to be exchanged, since they were only rated for wavelengths down to 300 nm. As it turned out, the power meter was also only rated down to 300 nm. A attempt to use a different power meter was made, however, the measurements highly innaccurate, and no further measurements were performed at this wavelength.

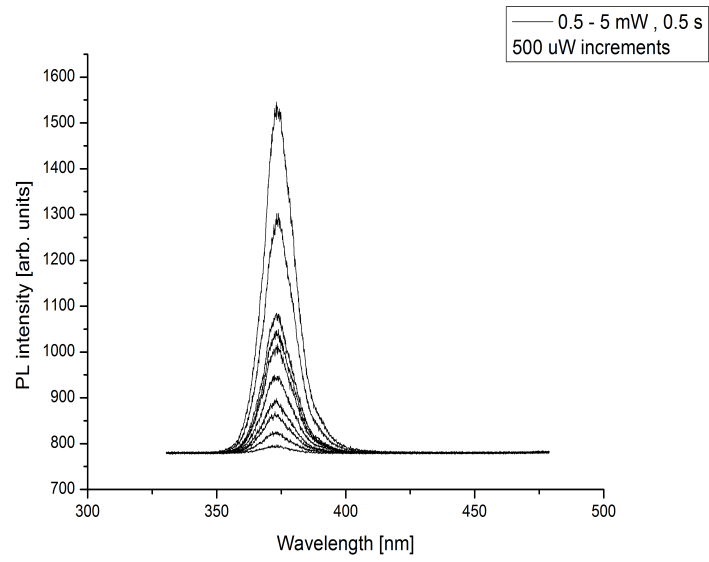


Figure 4.5: Pulsed laser illumination, 300nm, NW4

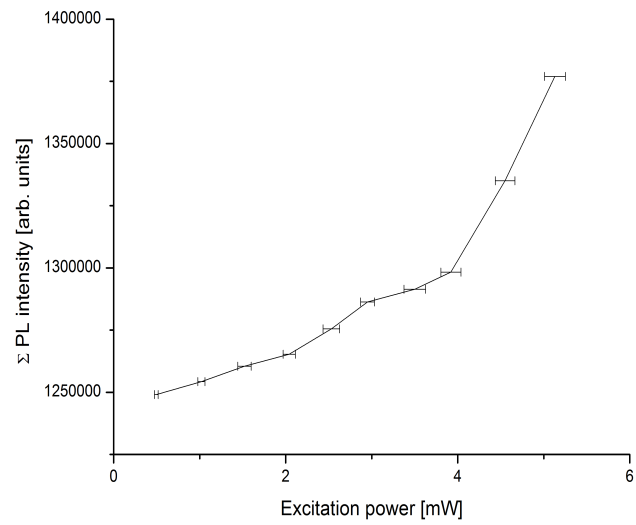


Figure 4.6: Power dependence, 300nm, NW4

## Chapter 5

# Conclusion

Although optically stimulated emission was not observed in the conducted experiments, possible signs of gain were present. As mentioned previously, these nanowires exhibit strong PL emission compared to the wires examined during my specialization project, and are a more viable candidate for achieving stimulated emission. If one were able to deliver more optical power to the wires[8], either pulsed or continuous, the observations in these experiments could be explored further. In addition, thanks to the new streak camera in the nanophotonics lab at NTNU, time-resolved spectroscopy and life-time measurements can be carried out to further analyze the properties of these nanowires.

# Bibliography

- [1] Yang, P., et al., “Controlled Growth of ZnO Nanowires and Their Optical Properties”, *Adv. Funct. Mater.* no. 5, 2002
- [2] Noh, J.H. et al., “Photoluminescence and electrical properties of epitaxial Al-doped ZnO transparent conducting thin films”, *Phys. Status Solidi A* 206, 2009
- [3] Fan., Z., Lu, J. G., “Zinc Oxide Nanostructures: Synthesis and Properties”, *Journal of Nanoscience and Nanotechnology*, 5(10), 1561-1573, 2005
- [4] Quirk, M., Serda, J., “Semiconductor Manufacturing Technology”, Prentice Hall, 2001
- [5] Cui, J. B., Thomas, M. A., “Power dependent photoluminescence of ZnO”, *Journal of Applied Physics* 106, 2009
- [6] Streetman, B.G., Banerjee, S.K., “Solid State Electronic Devices”, Prentice Hall , 2006
- [7] Kittel, C. “Introduction to Solid State Physics”, John Wiley & Sons, 2005
- [8] Zimmler, M. A., et al., “Laser action in nanowires: Observation of the transition from amplified spontaneous emission to laser oscillation”, *Appl. Phys. Lett.* 93, 051101, 2008

# Chapter 6

## Appendix

### 6.1 Power dependence and standard deviation

Table 6.1: NW1 power dependence, 310 nm excitation, 60 s average

$P_{av}$ [mW]	SD(P)[ $\mu$ W]	Peak intensity
1.97	439	1260
1.54	232	1150
0.931	165	990
0.523	84	870

Table 6.2: NW2 power dependence, 310 nm excitation, 60 s average

$P_{av}$ [mW]	SD(P)[ $\mu$ W]	Peak intensity
2.23	70	1800
1.50	31	1520
1.03	31	1280
0.511	23	980

Table 6.3: NW3 power dependence, 310 nm excitation, 60 s average

$P_{av}$ [mW]	SD(P)[ $\mu$ W]	Peak intensity
2.16	57	930
1.48	32	850
1.01	28	818
0.49	9	795

Table 6.4: NW4 power dependence, 310 nm excitation, 60 s average

$P_{av}$ [mW]	SD(P)[ $\mu$ W]	Peak intensity
1.98	51	820
1.54	34	810
1.01	22	802
0.49	12	794

Table 6.5: NW1 power dependence, 300 nm excitation, 60 s average

$P_{av}$ [mW]	SD(P)[ $\mu$ W]	Peak intensity
5.13	96.4	2800
4.55	81.0	2450
3.96	76.4	1900
3.52	44.1	1800
2.97	60.0	1600
2.54	61.5	1400
2.01	35.2	1200
1.51	30.8	1060
1.02	24.0	930
0.497	14.1	830

Table 6.6: NW2 power dependence, 300 nm excitation, 60 s average

$P_{av}$ [mW]	SD(P)[ $\mu$ W]	Peak intensity
4.89	107.8	2000
4.37	117.8	1850
3.95	116.9	1800
3.54	94.4	1640
2.93	88.3	1430
2.55	77.8	1280
2.04	69.7	1160
1.45	63.7	1000
1.02	42.9	925
0.512	29.9	826

Table 6.7: NW3 power dependence, 300 nm excitation, 60 s average

$P_{av}$ [mW]	SD(P)[ $\mu$ W]	Peak intensity
5.08	146.0	1510
4.50	118.2	1450
4.03	102.2	1370
3.46	96.5	1240
2.98	99.2	1120
2.54	89.1	1040
2.00	80.8	970
1.52	53.9	910
1.00	38.7	850
0.496	18.2	805

Table 6.8: NW4 power dependence, 300 nm excitation, 60 s average

$P_{av}$ [mW]	SD(P)[ $\mu$ W]	Peak intensity
5.13	121.8	1550
4.55	113.6	1300
3.92	117.1	1090
3.50	125.6	1050
2.95	81.1	1010
2.53	97.2	950
2.04	71.5	900
1.52	77.0	865
1.02	41.0	827
0.495	21.5	798

## 6.2 Photoluminescence spectroscopy measurements

### 6.2.1 Continuous wave measurements

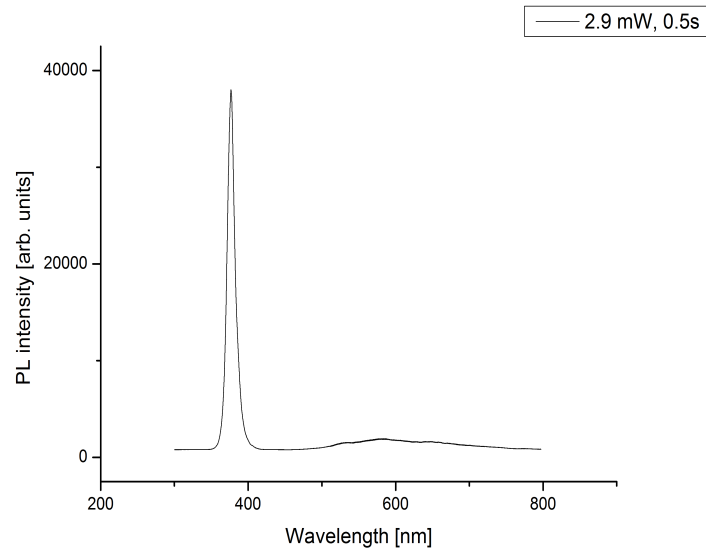


Figure 6.1: NW1, 11/11/11

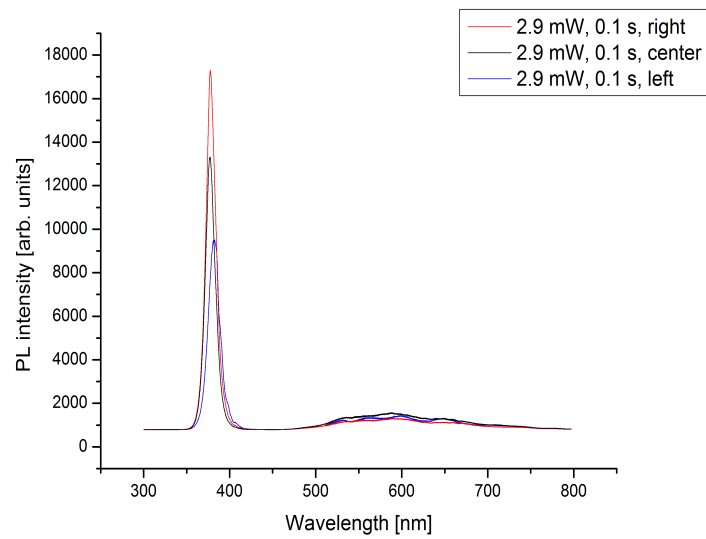


Figure 6.2: NW2, 11/11/11

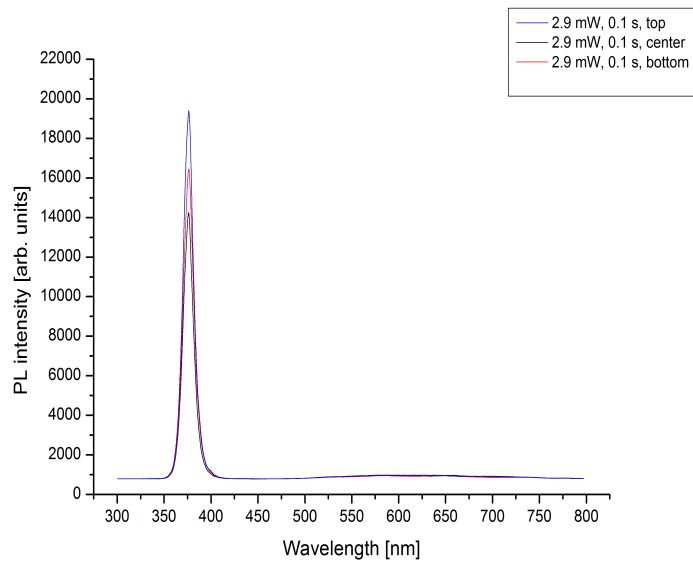


Figure 6.3: NW3, 11/11/11

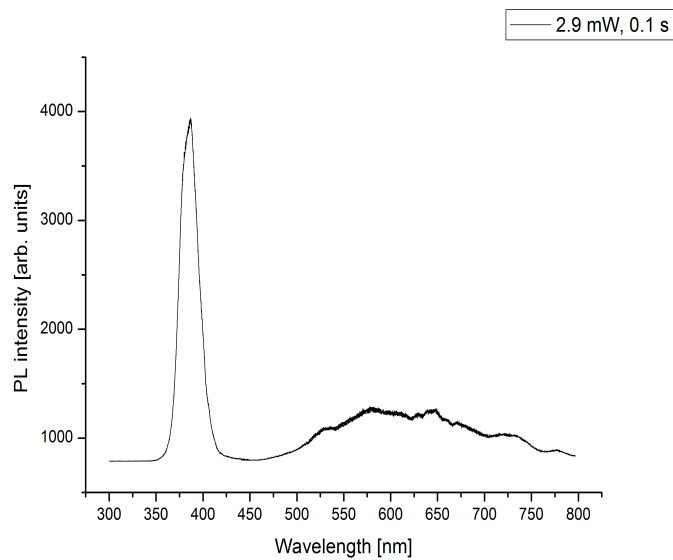


Figure 6.4: NW4, 11/11/11

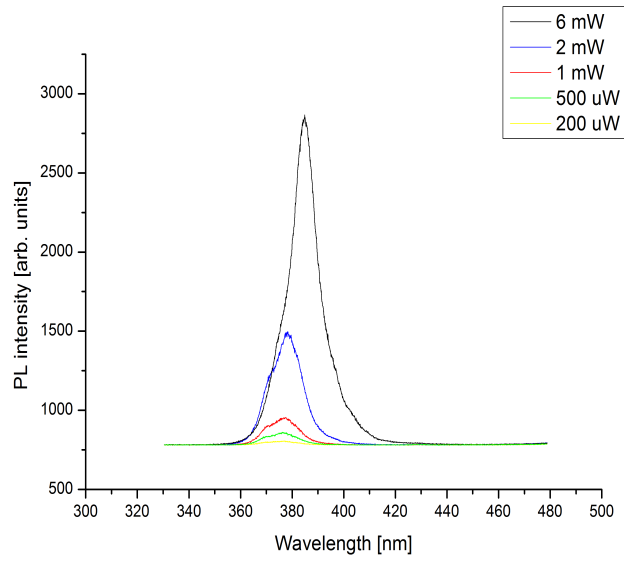


Figure 6.5: NW1 bottom, 19/01/12

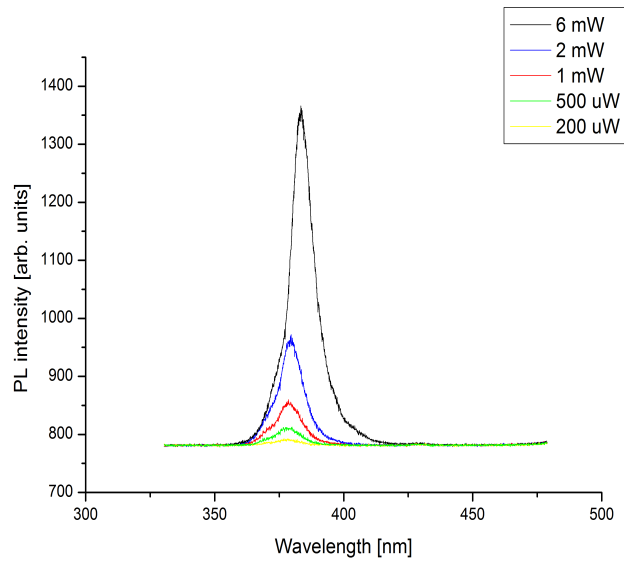


Figure 6.6: NW1 center, 19/01/12

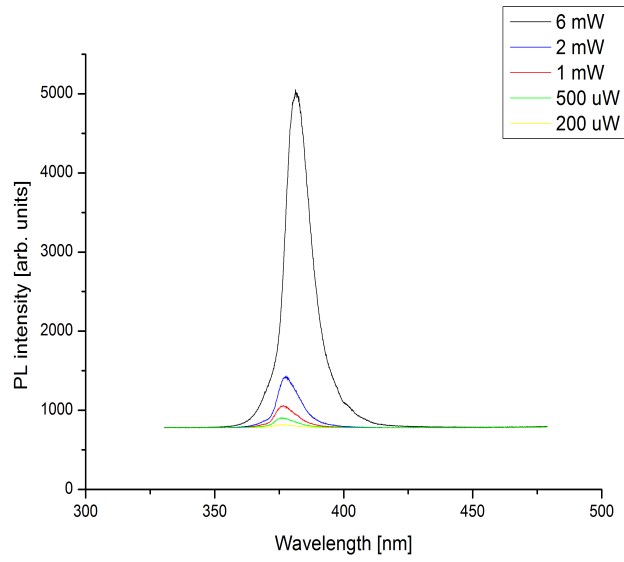


Figure 6.7: NW1 top, 19/01/12

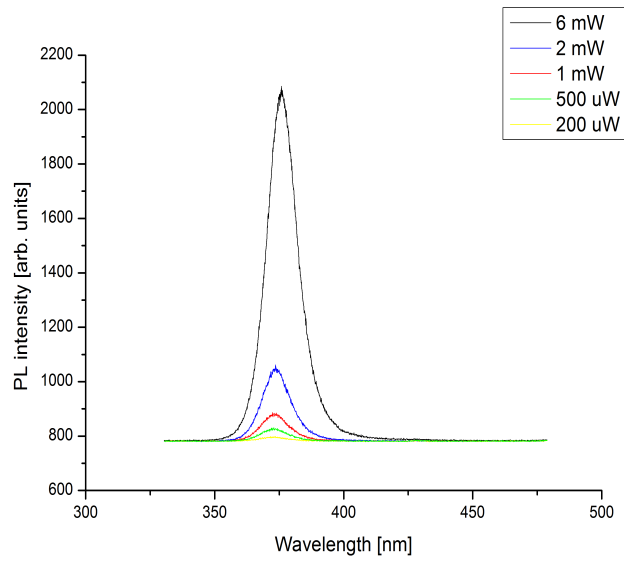


Figure 6.8: NW2 bottom, 19/01/12

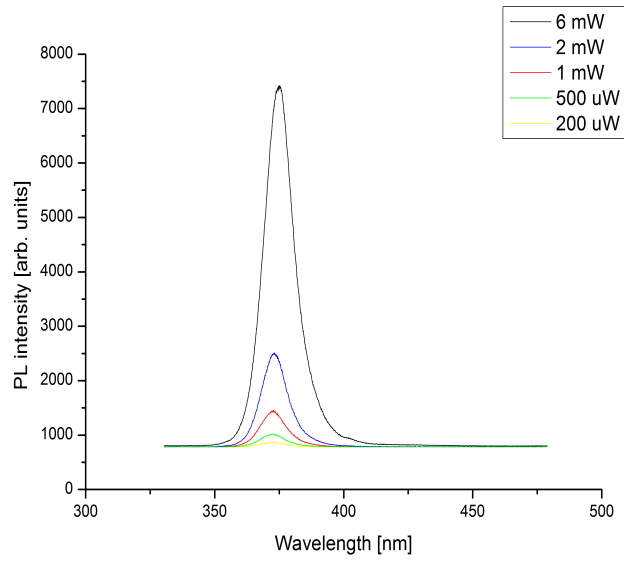


Figure 6.9: NW2 center, 19/01/12

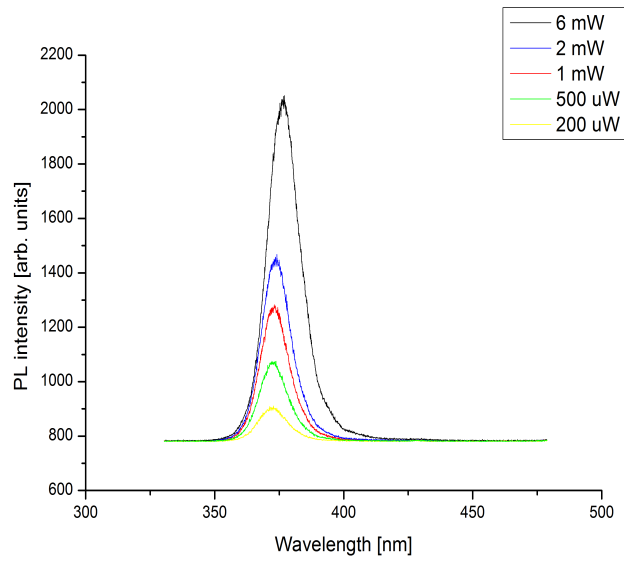


Figure 6.10: NW2 top, 19/01/12

## 6.2.2 Pulsed laser measurements

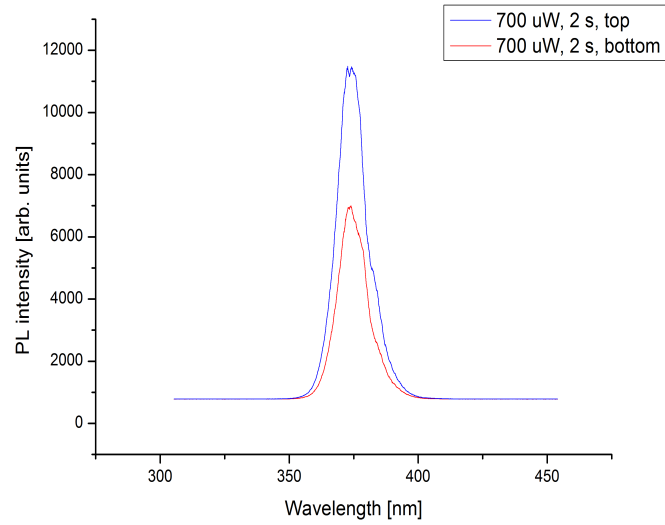


Figure 6.11: NW1, 310 nm excitation, 27/01/12

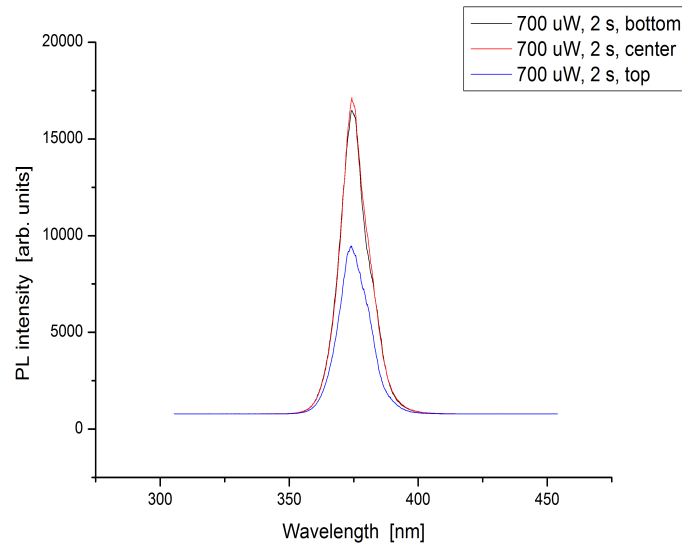


Figure 6.12: NW2, 310 nm excitation, 27/01/12

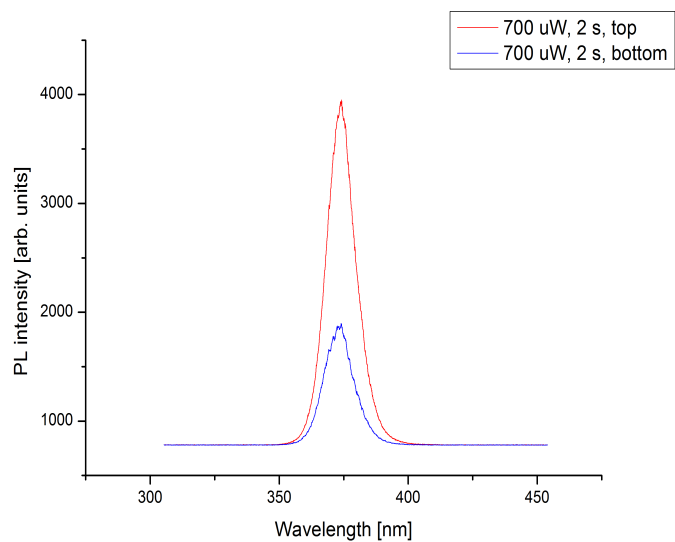


Figure 6.13: NW3, 310 nm excitation, 27/01/12

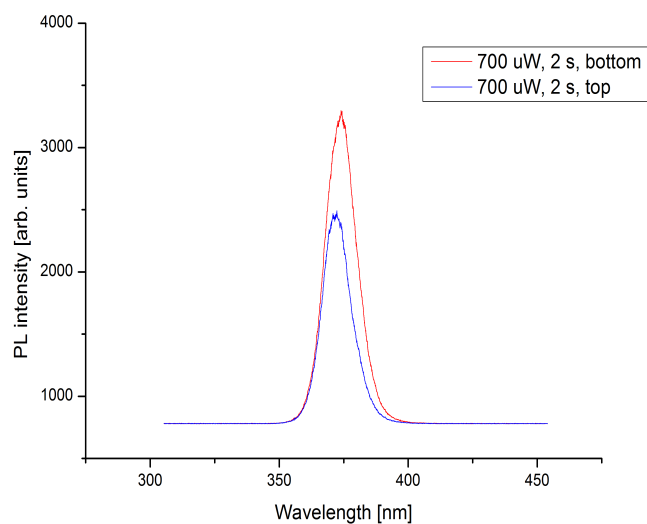


Figure 6.14: NW4, 310 nm excitation, 27/01/12